Mem. S.A.It. Suppl. Vol. 4, 9

Memorie della
Supplementi

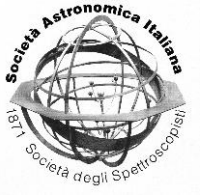

Adaptive Mesh Refinment simulations of jet formation

G. Bodo[1], C. Zanni[2], S. Massaglia[2], A. Ferrari[2], and P. Rossi[1]

[1] INAF - Osservatorio Astronomico di Torino, Italy e-mail: bodo@to.astro.it
[2] Dipartimento di Fisica Generale, Università di Torino, Italy

Abstract. We present MHD adaptive mesh refinment simulations of the process of acceleration and collimation of a jet from an accretion disk. The usage of the adaptive mesh refinment technique is dictated by the need of having good resolution both on the jet and on the disk, while considering a large integration domain for covering all the scales of interest. We discuss the acceleration and collimation processes and the roles of rotation and magnetic field in these processes.

Key words. jets – numerical simulations – adaptive mesh refinment

1. Introduction

The problems of how jets are accelerated and collimated are central for the understanding of the astrophysical jets phenomenon. There is now a general consensus that these processes are the result of an interplay between rotation and magnetic field. The magnetic field lines threading the accretion disk are carried by the rotating material and the matter outside the disk, sliding on the magnetic field lines, as in the "bead on the wire" analogy, is accelerated by the centrifugal force. Starting from the seminal paper by Blandford & Payne (1982), who first sketched this mechanism, a considerable theoretical effort has been spent on dealing with the stationary solutions of the MHD equations for modelling the outflow phenomena both from Active Galactic Nuclei and from Young Stellar Objects (see e.g. Lovelace, Berk, & Contopoulos 1991; Ostriker 1997; Krasnopolsky, Li, & Blandford 1999; Bogovalov & Tsinganos 1999; Casse & Ferreira 2000; Sauty, Tsinganos, & Trussoni 1999; Sauty, Trussoni, & Tsinganos 2002). These studies have pointed out the main effects involved in the acceleration and collimation processes. However, these solutions, due to the difficulty of the problem, have, in general, to make use of self-similar assumptions or to restrict to asymptotyc outflow properties (Heyvaerts & Norman 1989, 2003). Another line of approach is the use of numerical simulations, where, on the other hand, one has to face the problem of the large range of spatial and temporal scales involved. In principle, the timescales on which one would like to follow the process are much larger than the dynamical time scale of the system, that is fixed by the keplerian rotation period at the inner edge of the accretion disk. The first simulations of the process followed the evolution

Send offprint requests to: G. Bodo
Correspondence to: INAF - Osservatorio Astronomico di Torino, I-10025 Pino Torinese, Italy

only for few dynamical timescales and therefore essentially examined only transient phenomena (Shibata & Uchida 1986). Simulations performed more recently (Ouyed & Pudritz 1997; Ouyed, Clarke, & Pudritz 2003; Casse & Keppens 2002) follow the evolution over longer time scales trying to get a quasi steady behavior of the jet formation. Another limitation of some of the published simulations (see e.g. Ouyed, Clarke, & Pudritz 2003) is the treatment of the accretion disk simply as a boundary condition, while the interplay between jet and disk may be important in determining the dynamics. On the other hand, including the disk in the computational domain as it has been done for example by Casse & Keppens (2003), increases the computational cost, since, on one hand, one needs to keep a good resolution also on the disk, and, on the other hand, the domain of integation has to be large enough to allow to get information on the jet structure at large distances. For these reasons, the use of Adaptive Mesh Refinment techiques can lower the computational costs and we have therefore started a program of simulations using the public code FLASH (Fryxell et al. 2000) that implements these techniques. In the next section we will give some details about the numerical methods that we have used, in section 3 we will present our results, in section 4 we discuss the setup of our simulations and finally section 5 is devoted to summary and conclusions.

2. Numerical methods

The FLASH code (Fryxell et al. 2000), developed at the ASCI FLASH Center at the University of Chicago, is a public code for general astrophysical fluid-dynamics simulations. It is a is a state-of-the-art modular, adaptive mesh, parallel simulation code capable of handling general compressible flow problems found in many astrophysical environments and it is written in a modular way in order to facilitate its extension for including new physical processes. FLASH implements the approach to AMR known as block-structured AMR, through the use of the PARAMESH package (MacNeice et al. 2000). This approach make use of a hierarchy of logically cartesian grids and subgrids to cover the computational domain. In the original approach by Berger and collaborators (see e.g. Berger & Colella 1989) it is allowed for subgrids to overlap, to be rotated with respect to the coordinate axes, to have arbitrary shapes and to be merged with other subgrids at the the same refinment level, whenever appropriated. This strategy is flexible and efficient in term of memory occupation, but it results to be very complex to code and difficult to implement in a parallel environment. For these reason, several simplified approaches have been proposed, in particular DeZeeuw & Powell (1993) have proposed a variant in which the subgrid hierarchy is developed by bisecting grid blocks in each coordiante direction and linking them as the node of a data tree. This approach is very similar to that used by PARAMESH.

Some adaptations of the FLASH code have been however necessary for its application to our problem. In particular, our simulations need the usage of cylindrical coordinates with axisymmetry, but the distributed version of the FLASH code allows only for cartesian coordinates. Therefore we had to introduce the necessary correction for the correct implementation of the AMR scheme in cylindrical coordinates.

The MHD solver that we used belongs to the class of high resolution Godunov schemes that are the best suited for the treatment of supersonic flows. These schemes are based on a high order reconstruction of the variables in each cell and on an exact or approximate Riemann solver to be used at the cell interfaces for computing the fluxes. We made use of a linear reconstruction, giving second order spatial accuracy, coupled with an HLLE solver, that is an aproximate linearized Riemann solver, that assumes a-priori a two-wave configuration for the solution.

3. Numerical setup

We start our simulation with a cold and dense keplerian disk surrounded by a hot rarefied corona in gravitational equilibrium with the potential of a pointlike central object. The rotating disk is modelled following Abramowicz,

Jaroszynski, & Sikora (1978), (see also Kato, Kudoh, & Shibata 2002). The keplerian rotation law is defined by $v_\phi = v_{\rm k0}(r/r_0)^\beta$ ($\beta = -0.5$) where $v_{\rm k0} = (GM/r_0)^{1/2}$ is the keplerian speed evaluated at the cylindrical radius $r = r_0$ that is assumed as our unit of length and M is the mass of the central object. The disk density $\rho_{\rm disk}$ is defined as

$$\rho_{\rm disk} = \rho_{\rm d0}\left\{\frac{\gamma-1}{\gamma\alpha_{\rm d}}\left[\frac{r_0}{(r^2+z^2)^{1/2}}+\right.\right.$$
$$\left.\left.+\frac{1}{2\beta}\left(\frac{r}{r_0}\right)^{2\beta}+\Phi_0\right]\right\}^{\frac{1}{\gamma-1}} \quad (1)$$

where $\gamma = 5/3$ is the adiabatic exponent, $\alpha_{\rm d} = c_{\rm d0}^2/\gamma v_{\rm k0}^2 = 0.005$ is the ratio between the squares of the disk adiabatic sound speed $c_{\rm d0}$ and the keplerian speed evaluated at the point ($r = r_0$, $z = 0$). The constant Φ_0 is determined by requiring that $\rho_{\rm disk} = \rho_{\rm d0}$ at ($r = r_0$, $z = 0$). The equilibrium pressure is obtained assuming the polytropic relation $P_{\rm disk} = K\rho_{\rm disk}^\gamma$ where $K = v_{\rm k0}^2\rho_{\rm d0}^{1-\gamma}\alpha_{\rm d}$. The atmosphere above the disk is isothermal and in gravitational equilibrium with the potential of the central object. In order to avoid the singularity at the origin, the gravitational potential is smoothed with a quartic spline inside the spherical radius $R = (r^2+z^2)^{1/2} < 0.2r_0$. The density profile is therefore given by (for $R > 0.2r_0$)

$$\rho_{\rm atmo} = \rho_{\rm a0}\exp\left[\frac{1}{\alpha_{\rm a}}\left(\frac{r_0}{R}-1\right)\right] \quad (2)$$

where $\rho_{\rm a0} = 0.008\rho_{\rm d0}$ is the density in the corona evaluated at $R = r_0$, while $\alpha_{\rm a} = c_{\rm a}^2/\gamma v_{\rm k0}^2 = 1$ is the ratio between the squares of the atmosphere adiabatic sound speed $c_{\rm a}$ (which is a constant) and the keplerian speed evaluated at the point ($r = r_0$, $z = 0$). The equilibirum pressure of the hot corona is given by $P_{\rm atmo} = K\rho_{\rm atmo}$ where $K = v_{\rm k0}^2\alpha_{\rm a}$. The surface of the disk is given by the points where $P_{\rm atmo} = P_{\rm disk}$. Because of this surface condition the inner boundary of the disk is located approximately at $r = 2r_0$. The initial magnetic field is uniform, parallel to the axis of rotation of the disk and in equipartition with the thermal pressure of the disk that is $B_{\rm z0}^2/2 = \alpha_{\rm d}\rho_{\rm d0}v_{\rm k0}^2$. The computational domain has a size $r_{\rm domain} \times z_{\rm domain} = 20r_0 \times 80r_0$. We imposed to the AMR algorithm a maximum of 7 levels of refinement and, with 8×8 cell blocks, this is equivalent to a maximum resolution of 512×2048 grid points. In order to show how the Adaptive Mesh is able to increase the resolution only where required by the dynamics, we show in Fig. 1 four snapshots of the evolution of the system at different times with the adaptive grid superimposed. We adopted reflecting boundary conditions on the disk midplane and on the $r = 0$ boundary, outflow conditions (null gradient) on the outer boundaries apart from the outer part of the disk where the initial conditions for the disk are copied with a free outflow condition for the poloidal components of velocity and magnetic field. We also defined an internal boundary inside the region $R < 0.2r_0$ where the initial conditions of the hydrostatic atmosphere were kept fixed with a mass sink condition ($v_{\rm r} = \min(v_{\rm r}, 0)$, $v_{\rm z} = \min(v_{\rm z}, 0)$) on the poloidal velocity. In the following discussion the lengths will be given in units of r_0, the speeds are normalized in units of $v_{\rm k0}$ and the densities in units of $\rho_{\rm d0}$. In these units the period of rotation of the disk at $r = r_0$ is therefore equal to 2π.

4. Results

We followed the evolution of the system up to a time $t = 160$, equivalent to about 25 turns of the inner part of the disk and in Fig. 2 we show, at four different times, density maps with superimposed magnetic field lines. We can see that, starting from the initial conditions described above, we were able to produce a robust outflow. In the first panel we have the initial configuration, in the second panel we can observe that, as time elapses, the magnetic field lines open up, thus creating the favourable conditions to launch the outflow through the magnetocentrifugal mechanism described by Blandford & Payne (1982). This opening is due to the accretion motion of the disk, started by the extraction of angular momentum through torsional Alfven waves originated by the differential motion between the rotating disk and the steady atmosphere. In the third panel we

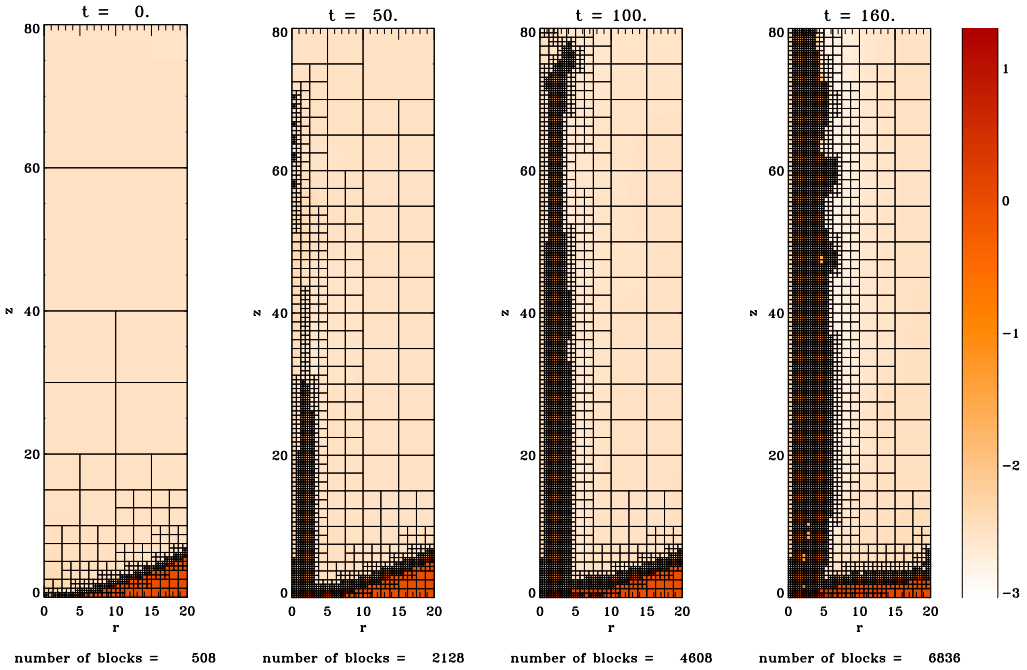

Fig. 1. The four panels show the distribution of the logarithm of density at four different times, with the adaptive grid superimposed

have a well formed collimated outflow, whose further evolution is shown in the fourth panel, where we can observe the formation of knotty fatures that will be further discussed below. In the next subsections we will discuss separately in more detail the acceleration, the collimation and the jet properties.

4.1. Acceleration mechanism

In order to show in detail how the outflow has been accelerated we plot in Fig. 3 cuts of the main driving forces along the z axis, in correspondence of the radius $r = 3$, at the time $t = 160$ of our simulation. In the first panel on the left we see that only the gradient of thermal pressure (dashed line) acts in order to support the disk against the gravitational acceleration (dotted line) and the magnetic pinch (solid line). But we can also notice that the Lorentz force change sign at the surface of the disk thus resulting as the main driving force that accelerates the jet. In the central panel we decompose the magnetic force (solid line) in its components $-J_\phi B_r$ (dashed line) and $J_r B_\phi$ (dotted line): it is possible to notice that both components change their sign at the disk surface or immediately above it; this effect, as noticed before by Ferreira & Pelletier (1995) and Casse & Keppens (2002) is due to the change of sign of the currents J_ϕ (mainly given by $\partial B_r/\partial z$) and $J_r = \partial B_\phi/\partial z$. Therefore the launching process seems to be associated with the gradient of the magnetic pressure $B_r^2/2 + B_\phi^2/2$ even if the gradient of the r component seems to be dominant. It is also important to take into account the toroidal Lorentz force plotted in the third panel (solid line): as we can see the effect of this force is a braking of the disk and a transfer of angular momentum from the disk to the jet, which is then centrifugally accelerated. Decomposing the toroidal force in its components $J_z B_r$ (dashed line) and $-J_r B_z$ (dotted line) we can see that the sign of the force is mainly due to the sign of the J_r current.

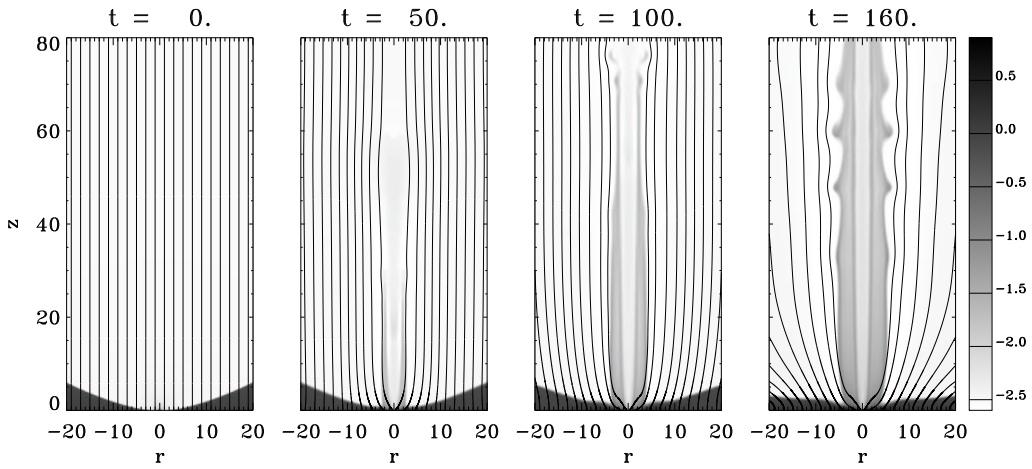

Fig. 2. The four panels show the distribution of the logarithm of density, at four different times, with superimposed the magnetic field lines. Notice that, respect to Fig. 1, we have replicated on the left the computational domain using the symmetry condition.

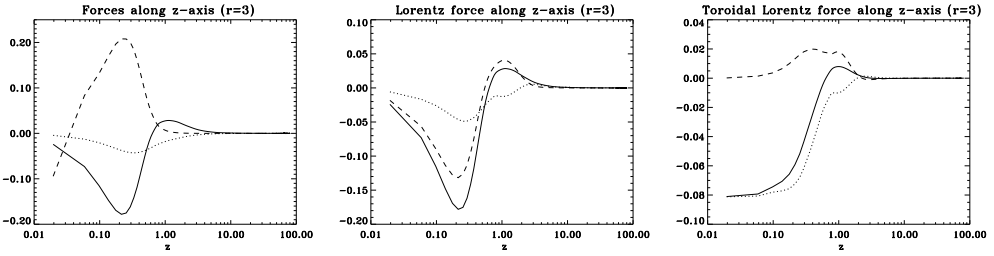

Fig. 3. Plots of vertical components of forces, computed at $r = 3$, as functions of the z coordinate. The left panel shows the Lorentz force (solid line), the thermal pressure (dashed line), and the gravitational acceleration (dotted line). The middle panel shows the Lorentz force (solid line) and its two components. The right panel shows the toroidal Lorenz force (solid line) and its two components.

4.2. Collimation of the outflow

In order to show how the accelerated outflow is collimated into a jet we plot in Fig. 4 (first panel on the left) cuts along the radial direction, at $z = 5$, of the radial components of the forces: as we can see both the thermal pressure gradients (dashed line) and centrifugal forces (dotted line) act so as to decollimate the flow while only the magnetic force (solid line) tends to collimate it. In the second panel we have decomposed the Lorentz force (solid line) into its components $-0.5\partial B^2/\partial r$ (dotted line) and $-B_\phi^2/r$ (dashed line): we can see that also the magnetic pressure tends to widen the outflow while the magnetic "hoop stress" ensures the collimation. The magnetic pinch associated with B_ϕ seems to be also responsible, togheter with centrifugel effects, for the formation of the knots that appear at later times along the jet. In Fig. 5 we show on the left these knotty features, while on the right we plot cuts, along the z direction, of the absolute value of magnetic "hoop stress" (dashed line) and the centrifugal force (solid line): we can see that, in correspondence of the knots (marked by letters A, B and C), we find the maximums of the pinching Lorentz force which tends to recolli-

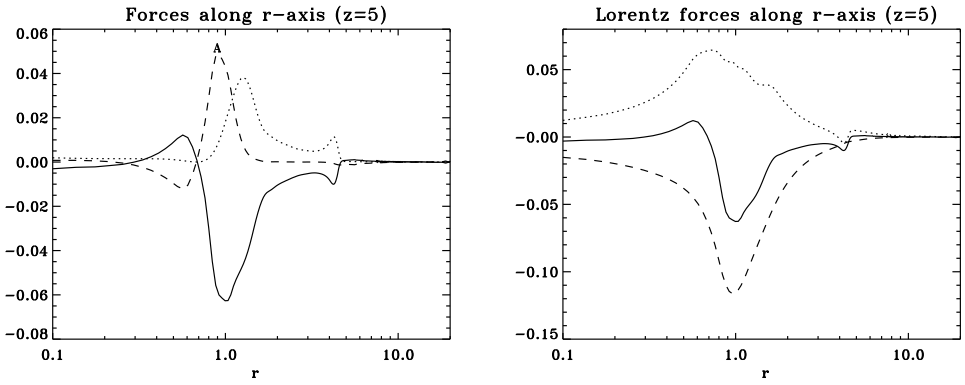

Fig. 4. Plot of the radial components of forces, computed at $z = 5$, as functions of the radial coordinate. The left panel show the Lorentz force (solid line), the thermal pressure gradient (dashed line) and the centrifugal force (dotted line), the right panel show the Lorentz force (solid line) and its two components.

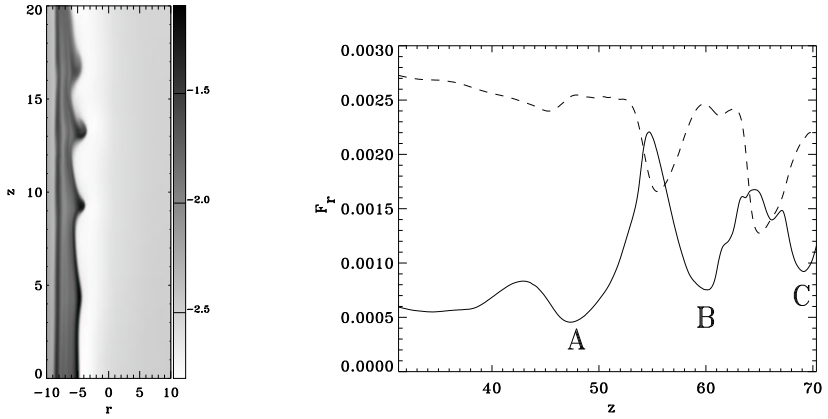

Fig. 5. The left panel show an image of the density distribution in which it is possible to observe the three knots discussed in the text. The right panel is a plot of the radial components of the Lorentz force (dashed line) and of the cetrifugal force, computed at $r = 3$, as functions of the vertical coordinate z. The knot positions are marked by the letters A, B and C.

mate the jet while, between them, the centrifugal barrier tends to widen the flow. This oscillating pattern is similar to what has been found in the simulations by Ouyed & Pudritz (1997) and in the steady analytical models by Sauty, Trussoni, & Tsinganos (2002).

4.3. Energy and mass flux

The jet launched in our simulation reaches a terminal asympotic speed around $1.2v_{\rm k0}$, thus approximatively around the escape speed from the potential well, and its matter has been accelerated to a mildly superfast magnetosonic flow speed. In the first panel in Fig. 6 we show the critical Alfvenic surface (dotted line) and fast magnetosonic surface (dashed line) while in the second panel a cut of the energy fluxes along the z direction at a radius $r = 3$ is shown: we can see that while on the disk scale the Poynting flux $= (B_\phi^2 + B_r^2)V_z - (V_r B_r + V_\phi B_\phi)B_z$

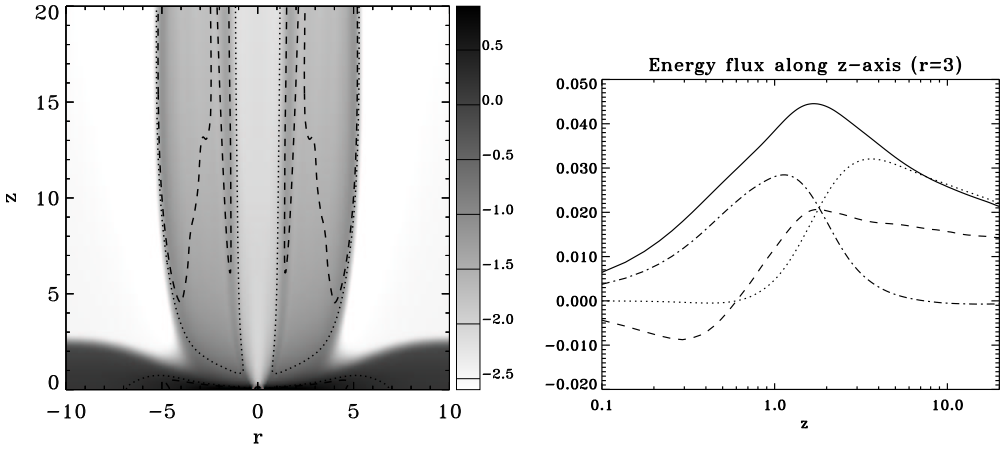

Fig. 6. The left panel shows an image of the inner part of the density distribution, at the final time of the simulation, with superimposed the positions at which becomes super-alfvenic (dotted line) and super-fastmagnetosonic (dashed line). The right panel shows a plot of the vertical energy fluxes, computed at $r = 3$, as functions of the vertical coordinate z. The solid line represents the Poynting flux, the dashed line represents the kinetic energy flux and the dotted and dashed-dotted ines represents th two omponents of the Poynting flux.

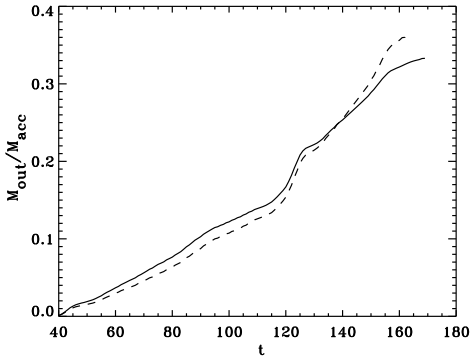

Fig. 7. Plot of the ratios between mass outflow rate in the jet and mass inflow rate in the disk (solid line) and angular momentum outflow rate in the jet and angular momentum inflow in the disk (dashed line) as functions of time.

(solid line) is dominant with respect to the kinetic flux = $1/2\rho v^2 v_z$ (dashed line), that around the midplane is even negative since the disk is accreting. But, at the end of our computational domain, these fluxes become comparable since, as said before, the terminal speed of the flow is mildly super-fastmagnetosonic. It is also interesting to notice that on the disk scale the Poynting flux is mainly due to the $-V_\phi B_\phi B_z$ component (dashed-dotted line), i.e. to the energy transported by the torsional Alfven waves which are extracting angular momentum from the disk; on the other the $B_\phi^2 V_z$ component (dotted line) due to the advection of the toroidal field becomes dominant along the outflow.

Finally in Fig. 7 we show the temporal behaviour of the ratio between the mass (solid line) and angular momentum (dotted line) outflow ($M_{\rm out}$) and accretion ($M_{\rm acc}$) rates as calculated on the surface of a cylinder of radius $r = 10r_0$ and heigth $z = 6r_0$. We can see that the two ratios are quite similar and quite high and do not tend to an asymptotic value thus ruling out the possibility that the system has reached a steady state. These effects can be due to the fact that in our calculations we didn't take into account resistive effects (apart from the numerical one) which are needed in order to obtain a steady accretion motion (Ferreira & Pelletier 1995).

5. Summary

We have performed MHD numerical simulations, with Adaptive Mesh Refinment, of the acceleration and collimation of a jet from an accretion disk. We used the public code FLASH with some modification, in order to make it suited to our configuration. These simulations allowed us to investigate in detail the mechanism at work in the acceleration and collimation of the jet. In particular we have discussed how the acceleration results from a combined effect of the magnetocentrifugal mechanism and of the gradient of magnetic pressure, while the collimation is the result of the action of the magnetic "hoop stresses". We have followed the evolution of the system for 25 rotation periods of the inner part of the disk and we found that, during this time, the ratio between the mass outflow rate in the jet and the mass inflow rate in the disk grows up to a value of about 30% and keeps increasing. Therefore the system does not seem to have reached a steady situation. A longer time integration and probably the inclusion of resistive effects are therefore needed for getting the steady long time properties of jets accelerated by accretion disk.

Acknowledgements. This work was partly supported by MIUR under grant COFIN-2002028843. The software used in this work was in part developed by the DOE-supported ASCI/Alliance Center for Astrophysical Thermonuclear Flashes at the University of Chicago. C.Z. thanks the University of Chicago for partly supporting his visit. The numerical calculations have been performed at CINECA in Bologna, Italy, thanks to the support of INAF.

References

Abramowicz, M., Jaroszynski, M., & Sikora, M. 1978, A&A, 63, 221
Berger, M. J. & Colella, P. 1989, Journal of Computational Physics, 82, 64
Blandford, R. D. & Payne, D. G. 1982, MNRAS, 199, 883
Bogovalov, S. & Tsinganos, K. 1999, MNRAS, 305, 211
Casse, F. & Ferreira, J. 2000, A&A, 361, 1178
Casse, F. & Keppens, R. 2002, ApJ, 581, 988
Casse, F. & Keppens, R. 2003, ArXiv Astrophysics e-prints, astro-ph/0310322
de Zeeuw, D., & Powell, K. G. 1993, J. Comput. Phys., 104, 56
Ferreira, J. & Pelletier, G. 1995, A&A, 295, 807
Fryxell, B. et al. 2000, ApJS, 131, 273
Heyvaerts, J. & Norman, C. 1989, ApJ, 347, 1055
Heyvaerts, J. & Norman, C. 2003, ApJ, 596, 1270
Kato, S. X., Kudoh, T., & Shibata, K. 2002, ApJ, 565, 1035
Krasnopolsky, R., Li, Z., & Blandford, R. 1999, ApJ, 526, 631
Lovelace, R. V. E., Berk, H. L., & Contopoulos, J. 1991, ApJ, 379, 696
MacNeice, P. et al. 2000, Comput. Phys. Commun., 126, 330
Ostriker, E. C. 1997, ApJ, 486, 291
Ouyed, R. & Pudritz, R. E. 1997, ApJ, 484, 794
Ouyed, R., Clarke, D. A., & Pudritz, R. E. 2003, ApJ, 582, 292
Sauty, C., Trussoni, E., & Tsinganos, K. 2002, A&A, 389, 1068
Sauty, C., Tsinganos, K., & Trussoni, E. 1999, A&A, 348, 327
Shibata, K. & Uchida, Y. 1986, PASJ, 38, 631